Highlights on mantle deformation beneath the Western Alps with seismic anisotropy using CIFALPS2 data

Pondrelli Silvia[1], Salimbeni Simone[1], Confal Judith M.[1], Malusà Marco G.[2], Paul Anne[3], Guillot Stephane[3], Solarino Stefano[4], Eva Elena[4], Aubert Coralie[3], Zhao Liang[5]

[1] Istituto Nazionale di Geofisica e Vulcanologia, Sezione di Bologna, Bologna, Italy

[2] Department of Earth and Environmental Sciences, University of Milano-Bicocca, Piazza della Scienza 4, 20126 Milan, Italy

[3] Univ. Grenoble Alpes, Univ. Savoie Mont Blanc, CNRS, IRD, UGE, ISTerre, Grenoble, France

[4] Istituto Nazionale di Geofisica e Vulcanologia, ONT, Genova, Italy

[5] State Key Laboratory of Lithospheric Evolution, Institute of Geology and Geophysics, Chinese Academy of Sciences, Beijing, China

Correspondence to: Silvia Pondrelli (silvia.pondrelli@ingv.it)

Abstract. There are still open questions about the deep structure beneath the Western Alps. Seismic velocity tomographies show the European slab subducting beneath the Adria plate, but all these images did not clarify completely the possible presence of tears, slab windows, or detachments. Seismic anisotropy, considered as an indicator of mantle deformation and studied using data recorded by dense networks, allows a better understanding of mantle flows in terms of location and orientation at depth. Using the large amount of shear wave splitting and splitting intensity measurements available in the Western Alps, collected through the CIFALPS2 temporary seismic network, together with already available data, some new patterns can be highlighted and gaps left by previous studies can be filled. Instead of the typical seismic anisotropy pattern parallel to the entire arc of the Western Alps, this study supports the presence of a differential contribution along the belt, only partly related to the European slab steepening. A nearly NS anisotropy pattern beneath the external Western Alps, a direction that cuts the morphological features of the belt, is clearly found with the new CIFALPS2 measurements. It is however confirmed that the asthenospheric flow from Central France towards the Tyrrhenian Sea, is turning around the southern tip of the European slab.

1 Introduction

Seismic anisotropy has become a convincing study tool, mainly in the areas where recent and past geodynamic evolution have left their marks in the mantle deformation and its patterns (e.g. Long and Silver, 2009; Long, 2013 for a complete review). Several methods exist to measure seismic anisotropy. Depending on the used seismic phase, signal, and frequency, it is possible to measure seismic anisotropy at different depths and relate it to different parts of the Earth's structure, last but not least with seismic anisotropy tomography (e.g. Zhao et al., 2023). Local seismicity and surface waves are used to measure

crustal seismic anisotropy, usually attributed to fractures or/and the state of stress of crustal depths (i.e. Crampin and Peacock, 2008; Okaya et al., 2018). Using seismic signals that travel deeper, it is possible to sample the deformation at lithospheric-asthenospheric depths. For instance, Pn phases record the seismic anisotropy immediately below the Moho in the lithospheric mantle (i.e. Diaz et al., 2013). On the other hand, using core phases (SKS, SKKS, etc) that record information on the receiver branch of their path, we can sample seismic anisotropy that is thought to be mainly concentrated in the upper mantle.

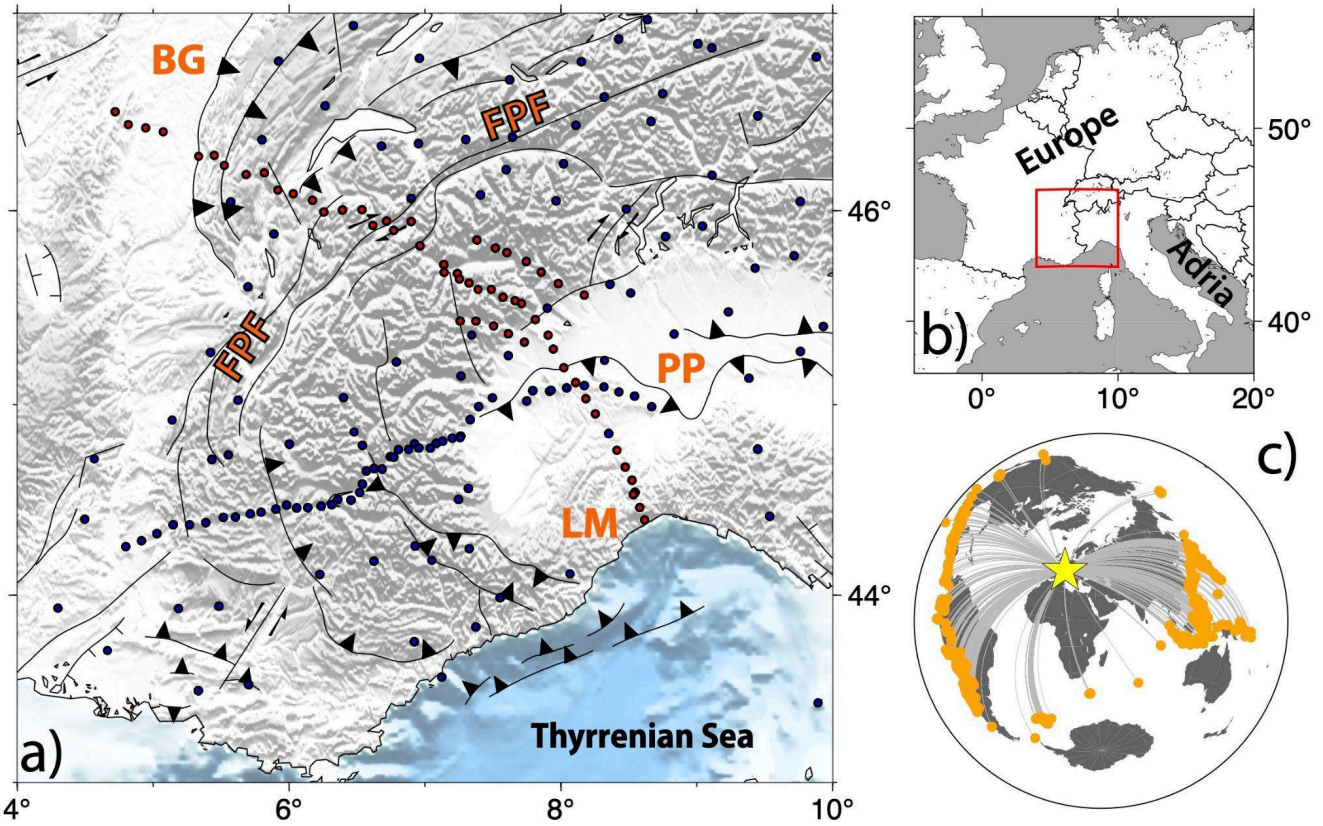

Figure 1 - a) Map of the study region, focusing on the Western Alps. In red are indicated the CIFALPS2 stations, while in blue are permanent and previous temporary stations (i.e. CIFALPS and AlpArray). FPF = Frontal Pennine Fault, BG = Bresse Graben, PP = Po Plain, LM = Ligurian Mountains; b) the red square is the study area reported in a); c) map of all seismic events used in this study, with the star centered in the study region.

The azimuth of the fast velocity direction and the delay time, the two parameters that commonly result from shear wave splitting analysis of core phases, are interpreted respectively as the direction assumed by olivine crystals, the principal mineral component of the upper mantle when mantle undergoes deformation, and the amount of anisotropy crossed by a seismic ray.

In the Alps these kinds of measurements improved immensely with recent temporary experiments such as AlpArray (Hetényi et al., 2018) or CIFALPS and CIFALPS2 in the western sector of the chain (Zhao et al., 2015; 2016: 2018), which complemented the permanent seismic networks operating in the region.

The European Alps originated in the late Cretaceous from the oblique subduction of the Alpine Tethys under the Adria microplate. The subduction evolved in a continental collision during the late Cenozoic (e.g., Handy et al., 2010, 2013 and references therein). In the Western Alps, the tectonic lineament that worked as the suture accommodating the shortening between the two plates is the Frontal Penninc Fault (FPF, Fig. 1). Even though the geological history of this belt is one of the best studied and well known in the world, the geodynamic evolution of the European slab, in terms of position and possible presence of slab break off, is still poorly understood.

All travel time tomographic studies identified at mantle depth the presence of seismic velocity heterogeneities interpreted as the European slab subducting beneath the Adria plate (e.g. Piromallo and Morelli, 2003; Lippitsch et al., 2003; Kissling et al., 2006; Giacomuzzi et al., 2011; Paffrath et al., 2021; Rappisi et al., 2022). However, the existence of possible slab detachments, windows or tears is debated, for instance beneath the Western Alps (e.g., Zhao et al., 2016). The first CIFALPS experiment (see Malusà et al., 2021 and references therein) clarified several points, starting from the first seismic evidence of subducted European continental lithosphere beneath the Adria lithosphere (Zhao et al., 2015), to a tomographic model with a continuous slab beneath this region (Zhao et al., 2016). In addition, recent seismic anisotropy analyses of the Western to the Central Alps shed additional light on potential discontinuities of the slabs, thanks to the possible mapping of mantle flows that would occur through them (Petrescu et al., 2020; Salimbeni et al., 2018).
The additional contribution of CIFALPS2, a temporary experiment deployed for 14 months from 2018 to 2019 (Zhao et al., 2018), on mantle seismic anisotropy mapping and interpretation, was expected to fill a gap in the northwestern part of the Alpine arc (red dots in Figure 1). Receiver function and ambient-noise tomography studies have underlined the north-south differences in the lithospheric structure along the belt strike (Paul et al., 2022). Therefore, there is a need for measuring additional seismic anisotropy in the mantle from CIFALPS2 data and to compare them to previous results.

In this study, we present the results of the analysis of data recorded by CIFALPS2, describing them in an integrated view with previous shear wave splitting measurements (SWS) to identify new features in the mantle and draw hypotheses on their origin.

2 Data and Methods

Data used for the analysis are the recordings at CIFALPS2 stations (Figure 1; Zhao et al., 2018; doi: 10.15778/RESIF.XT2018) of teleseismic earthquakes with a magnitude M>6.0, that occurred between June 2018 and

December 2019 and are located at a distance interval from the network between 88° and 120°, typical to guarantee well isolated SKS phases in the waveforms. 80 to 150 events for each of the 56 temporary stations have been analyzed (Figure 1).

The entire SWS analysis has been conducted using the code SplitRacer (Reiss and Rümpker, 2017), based on the Silver and Chan (1991) method and thus on the minimization of the energy on the transverse component. Different filters have been applied according to the amount of noise at the various sites. For most of them, located in the Alps or Ligurian mountains, a bandpass filter between 7 and 20 s worked well, while for instance sites in the Po Plain needed different choices, i.e. 5-30 s. The signal to noise ratio (SNR) was also used to avoid noisy waveforms; initially, the threshold was 3, but where the amount of events to be analyzed was scarce we decreased it down to 1.5, again mainly for sites located in or close to the Po Plain. It is worth noticing that SWS analysis recovers fast-velocity directions, assuming a single layer of horizontal anisotropy. Moreover, the depth at which this anisotropy is located is difficult to define, but it is classically assumed that most measured anisotropy is in the upper mantle (Savage, 1999). Thus, it is common to visualize any lateral variation by plotting results at the piercing point of the incident ray at 150 km depth (Figure 2a).

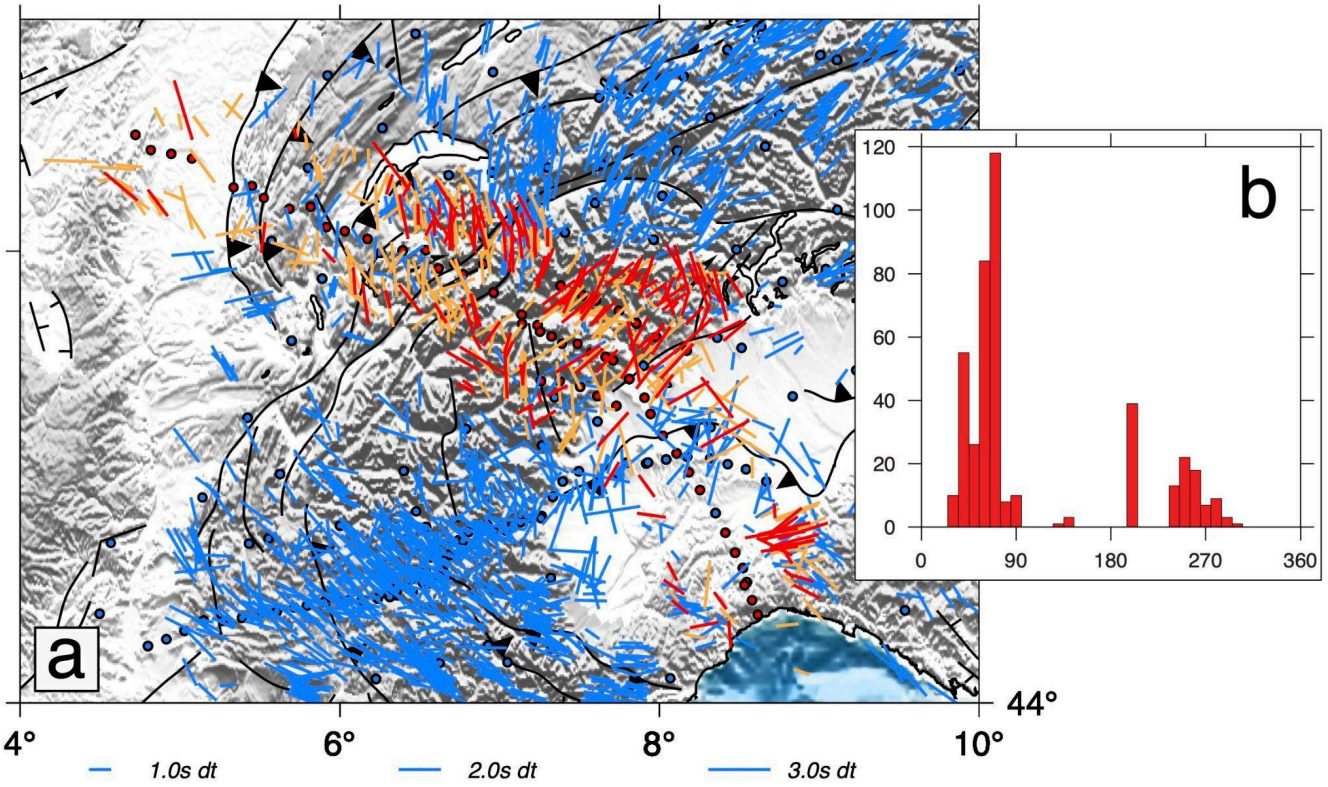

Figure 2 - a) Map of single SWS measurements for the study region, plotted at the location of the piercing point of the ray at 150 km depth. In red and orange are good and fair measurements from CIFALPS2 stations (red circles) respectively. In the background, in light blue, previous SWS measurements and stations; b) histogram of back azimuths of events used in the analysis.

To improve the resolution of the data to be discussed and interpreted, splitting intensity (SI) measurements have been performed on the same CIFALPS2 recordings used for SWS measures (Table S2 in Supplementary Material). Splitting intensity is measured by projecting the transverse component on the radial component derivative; it is related to the variations of the amplitude of the transverse component with the back azimuth (Chevrot, 2000; Monteiller and Chevrot, 2010). A routine based on Kong et al. (2015) and Confal et al. (2023) was used to calculate splitting intensity values from waveforms with a cut-off of 15 s before and 30 s after the supposed SKS arrival. A dominant period of 12 s is used for the Wiener filtering. To filter out low quality waveforms in this automatic process a cross-correlation coefficient of |0.7| and splitting intensities values and error threshold of |2.0| and 0.5 respectively were used (Baccheschi et al., under revision). With splitting measurements from at least four different 10° bins of back azimuths, the classical evaluation of the anisotropy parameters, i.e. the azimuth of the fast direction phi and the delay time dt, is obtained by fitting a sinusoid to the back azimuthal dependence of splitting intensity values (Chevrot, 2000). In particular, the sinusoid amplitude and phase give dt and phi respectively (see Figure S1 in Supplementary Material as an example).

3 Shear wave splitting results

From SWS analysis we obtained more than 400 pairs of splitting parameters (phi and dt) if we consider together good (170) and fair (241) results (Figure 2a, good in red, fair in orange; all results are available at https://osf.io/nqxk4, Pondrelli et al., 2023). The quality assignment is given following the SplitRacer criteria (Reiss and Rümpker, 2017), considering the visibility of the phase, the ellipticity of the initial particle motion and its linearity in the final stage, and the errors associated with phi and dt values. In Figure S2 of the Supplementary Material some measurement examples are shown. In addition, nearly 600 null measurements have been obtained (Figure S3 in Supplementary Material), where a null is considered when no split appears in the signal (i.e. no energy in the transversal component). This is due either to the absence of anisotropy or to the initial polarization being parallel to the fast or slow anisotropic direction. A high percentage of good and fair results were obtained for events with a NE back azimuth, so it should be taken into account that this direction is oversampled (Figure 2b).

This new dataset fills the region between the north-western external Alps and the Ligurian Sea. The anisotropy directions of no-nulls and nulls mostly agree with previous measurements (Figures 2 and 3, Figure S3 in Suppl. Material). Along the part of the transect crossing the Alps (transect AA' in Figure 3), NE-SW direction dominates in the internal part of the belt, between the FPF and the boundary of the Po Plain (see average values, red dots in Figure 3). In the western part of the AA' transect, measurements are more scattered, with a coexistence of NE-SW and NS to NNE-SSW directions. In the outer part of the Alpine belt and in the Bresse Graben, the prevailing directions are NS to NNE-SSW. Anisotropy in this region is weaker, but fast velocity directions remain constant toward the NW end of the transect, confirmed also by null measurements

(Fig.S3 in Supplementary Material). These two patterns, one NE-SW parallel to the Alps strike and the other nearly NS, and their location along the transect are well visible in Figure 3, mainly following average values (reddish dots).

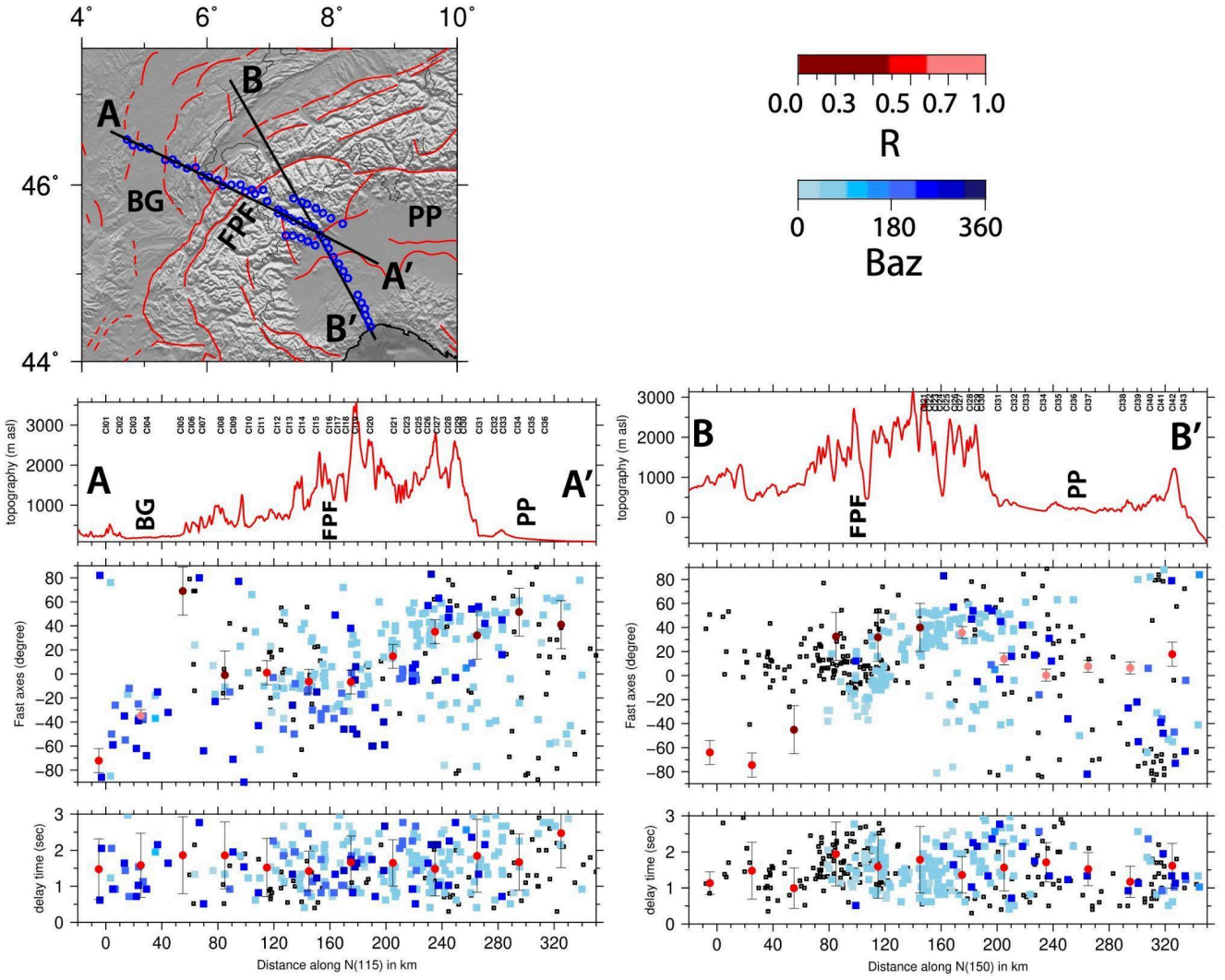

Figure 3 - Distribution of splitting parameters along the two sections of the CIFALPS2 region. For each section topography (upper), fast axes direction (middle) and delay time (lower) distributions along a swath box of 30 km are displayed. In the fast axes and delay time panels, every single measurement is represented by a square; the results of CIFALPS2 are blueish and color coded in agreement with the back azimuth of the events analyzed, while the results of previous works are represented by smaller empty squares. In the fast axes panel, circles represent the average values calculated using a basic circular arithmetic mean inside the swath box with 30-km-step increment; they are coloured in agreement with the spreading distribution around the mean value (R=0 distribution completely scattered, R=1 distribution completely aligned with the mean direction). In the delay time panels, red dots are the average value and its error, calculated with arithmetic mean and standard deviation. FPF = Frontal Penninic Fault; BG = Bresse Graben; PP = Po Plain.

In the Po Plain, measurements appear scattered, similar to previous studies (e.g. Salimbeni et al., 2018; Petrescu et al., 2020; Figures 2 and 3). In the transition between the belt and the plain, the typical NE-SW Alpine direction prevails. Even if measurements are scarce, this direction appears also in the center of the Po Plain, together with a few NW-SE directions located southeast, close to the Ligurian Alps. However section BB' in Figure 3 shows that anisotropy directions are diverse, resulting in a strong dispersion of average values computed along the section. In the Ligurian part of the transect, several directions are detected, ENE-SSW and NW-SE (Apenninic) on the eastern side with a few weaker (lower dt) NNE-SSW measurements in the western side.

In general, we do not find any particular pattern in the delay time measurements. Average values computed along the sections (Figure 3) are mostly constant, around 1.5 s with a large range in single measurement values.

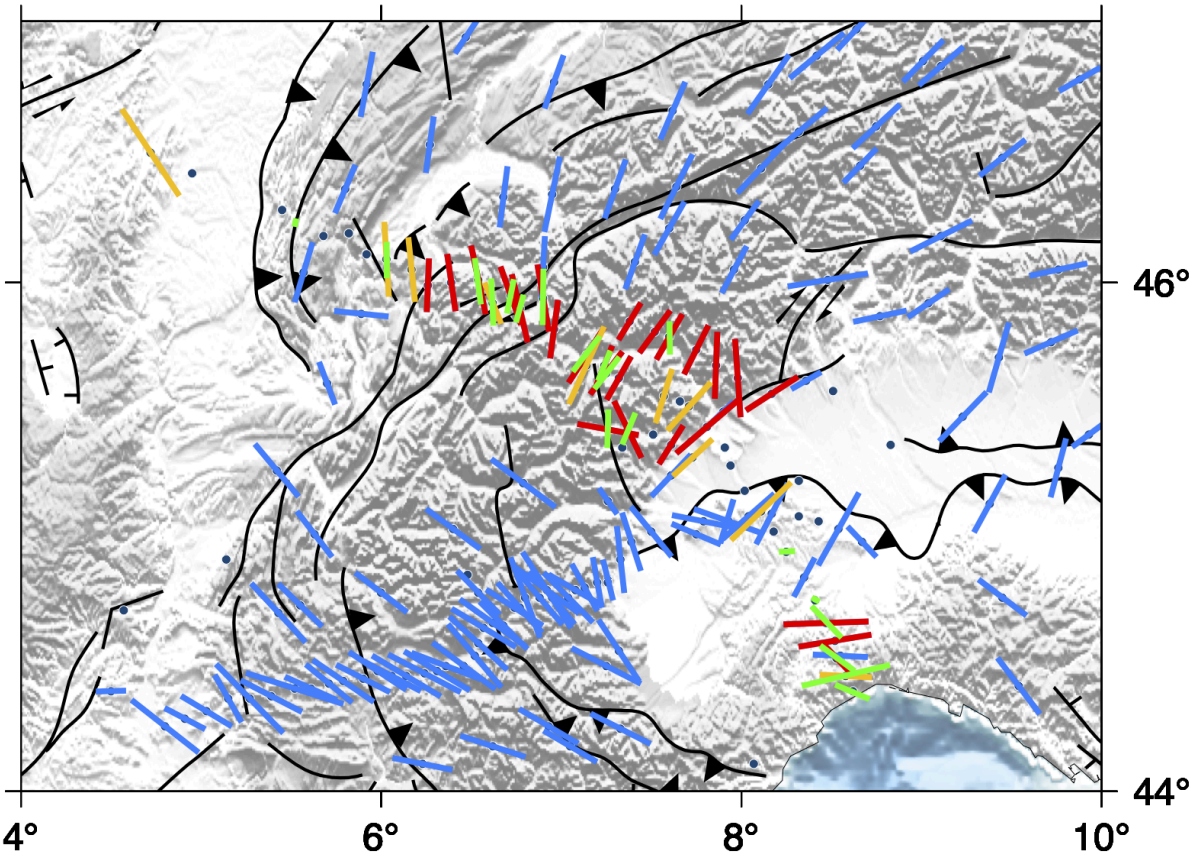

Figure 4 - Maps of average SWS measurements (red, yellow and blue) and anisotropy parameters obtained using SI measurements (green). In red average values for CIFALPS2 stations obtained with more than 3 measurements, in yellow averages obtained with less than 3 values; in light blue, average measurements from previous works. Dots represent stations.

In Figure 4, average SWS values for each station are mapped together with anisotropy values obtained by splitting intensity (SI) measurements (Table S1 in Supplementary Material). The first observation is that average SWS and SI data are very similar, mainly at sites where the single measurement results are more homogeneous, while differences are present where back azimuthal variations in fast direction are more evident, for instance in the southernmost part of the transect, in the Ligurian Mountains.

In general, it is clear that CIFALPS2 results are coherent with the average distribution of the anisotropy from previous measurements. The main Alpine pattern that follows the belt arc, here NE-SW, is represented in most of the averaged values for sites located in the transition between the Po Plain and the FPF. From the FPF to the NW endpoint of the transect, the main direction is close to NS, a direction that does not find an agreement with the orogen trend, still NE-SW.

In order to extract as much information as possible, we split the dataset into groups according to the main morphological features: a) External zone to the west of the FPF; b) Internal zone between the FPF and the western boundary of the Po plain, c) the Po Plain, and d) the Ligurian Alps. By plotting a rose diagram for all good and fair measurements obtained for the stations of each group, taking into account the influence of back azimuths, we get an overview of the main features and lateral changes of the anisotropy detected through these SWS measurements.

In Figure 5, the rose diagrams show evident differences along the CIFALPS2 transect, somewhere underlined by different patterns with respect to back azimuths. Only in group a), in the External zone, the N-S dominant direction remains, regardless of the amount of measurements or separation into opposite back azimuths (red and blue rose diagrams). For all other groups, there is a clear difference depending on the back azimuth. In group b) the entire dataset shows a main trend in a NE-SW direction, in agreement with the Alps strike in this region; the same direction is observed for events coming from NE (blue rose diagram). On the contrary, measurements obtained from events with a SW back azimuth are dominated by a nearly NS direction, quite similar to that shown by group a). The entire dataset for the Po Plain (c) and the subgroup with east back azimuths show a clear bimodal distribution, with both the Alpine NE-SW and the Apenninic NW-SE typical directions; west back azimuth events show instead N to NNW directions, very similar to those obtained in previous work at the first CIFALPS transect (e.g. Salimbeni et al., 2018) and again similar to group a) and SW back azimuth measurements of group b). In the Ligurian Alps, in the group d), opposite back azimuths show different results. It is worth noticing that in the group d) the ENE-WSW direction is dominant both in the all data plot and in the east back azimuth plot, while the west back azimuth plot shows a wide dispersion with a NW-SE direction prevailing.

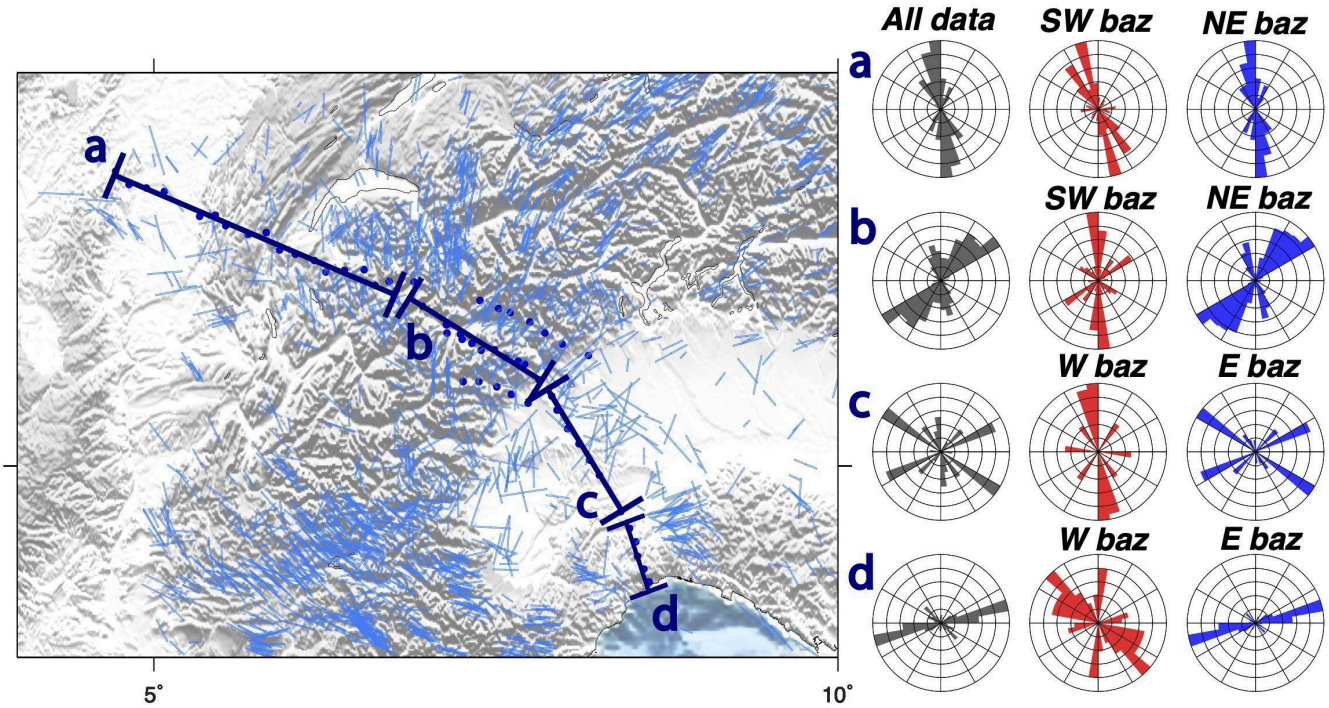

Figure 5 - Normalised rose diagrams produced for groups of stations along the profile, a) External zone with respect to FPF; b) Internal zone with respect to FPF; c) Po Plain; d) the Ligurian Alps. Grey rose diagrams: all data; Red: events with SW (a,b) or W (c,d) back azimuths, blue: events with NE (a,b) or E (c,d) back azimuths.

4 Discussion and hypotheses

CIFALPS2 SWS measurements clearly provide new information since they cover large areas where no seismic station is currently deployed or has been operating in the past. They allow us to fill data gaps and draw conclusions on the seismic anisotropy pattern and mantle deformation beneath the Western Alps.

A large-scale summary, prepared using the average values to avoid the scatter of single SWS measurements, is shown in Figure 6. ENE-WSW fast velocity directions, parallel to the strike of the Alps, are present from the Central to the Western Alps, in the transition between Po Plain and the belt, and terminate where the European slab and the belt are bending (double headed arrows in the inset sketch of Figure 6). At this point anisotropy directions do not strictly follow the chain strike, as they rather cut the main tectonic and morphological features. In the same zone (highlighted by the green circle A, Figure 6) converges a mantle flow that strikes from NE-SW to NS, in a coherent direction that however cuts the arcuate shape of the belt (yellow lines in the northern part of study region, Figure 6); this pattern is different from those described in previous anisotropy studies of the Western Alps (Barruol et al., 2004; Lucente et al., 2006; Barruol et al., 2011; Salimbeni et al., 2018)

where anisotropy has always been described as rotating with the belt direction. The discrepancy between the direction of tectonic lines and the nearly NS fast velocity is in agreement with a deep source of the anisotropy, in the mantle. Link and Rumpker (2023) in a recent analysis found that a similar nearly NS pattern would be mostly located in a shallower part of the mantle, and in part also present in a lower layer. They consider it as a shallow asthenospheric contribution.
On the contrary, the NW-SE asthenospheric flow identified from SE France toward the Ligurian Sea, which culminates in a flow around the southern tip of the European slab, is in agreement with previous studies. This flow apparently originates beneath Central France, in the Massif Central region (Barruol et al., 2004), and it seems that the NS mantle flow merges with it (left green circle, Figure 6) and then, flowing around the southern tip of the European slab, moves to the Tyrrhenian Sea.

The overlap with the teleseismic travel time tomographic image at 150 km depth by Zhao et al. (2016) indicates that all these fast velocity directions correspond to mantle deformation below the European slab. The mantle close to the slab has a NE-SW seismic anisotropy direction because it is deformed by the slab steepening. This feature is visible only in a narrow stripe, in the transition between Western and Central Alps, probably because in this place the slab steepening was favored by the plate motion direction (e.g. Adria anticlockwise rotation, Figure 6). Moving north, in the outer part of the belt, the anisotropy directions are those of an undeformed mantle, substantially parallel to the APM direction (orange arrows in Figure 6). Moving (south)westward, the deflection from NE-SW to NS may be related to the mantle being squeezed by the retreating European slab and moved toward the south where the retreat process was weakening or probably already ended. Indeed, in the Western Alps, the arcuate shape of the trench and slab, together with the (upper) Adria plate rotating in anticlockwise direction with a rotation pole more or less located in the western Po Plain (e.g. Serpelloni et al., 2016; Le Breton et al., 2017), may have been less favorable to the retreat of the slab. Such differences between the northern and southern Western Alps, in particular in the European Moho geometry, have been also identified by comparing CIFALPS and CIFALPS2 receiver function sections (Paul et al., 2022). The European Moho is strongly dipping down to ~75 km depth along CIFALPS section, while its dip is much weaker in CIFALPS2 section. Moreover, the absence of slab retreat in the Western Alps has been described also by Malusà et al. (2015), studying the mechanisms for exhumation of (U)HP terranes along the Cenozoic Adria-Europe plate boundary.
The mantle flow from beneath the Central Alps converges with the asthenospheric flow coming from SE France where Western Alps subduction, precisely a continental subduction (Malusà et al., 2021; Paul et al., 2022) runs out. In the region, the European slab is almost vertical (Zhao et al., 2016) and is no more affected by slab retreat. Substantially a differential behaviour of slab movement along the chain is at the base of the anisotropy pattern variation from Central to the entire Western Alps.
In the Po Plain, the image is patchy and complex, with very few good quality measurements and some really low values of dt. This does not necessarily mean that the mantle is isotropic, but that anisotropy may be multilayered or fast velocity directions are vertical.

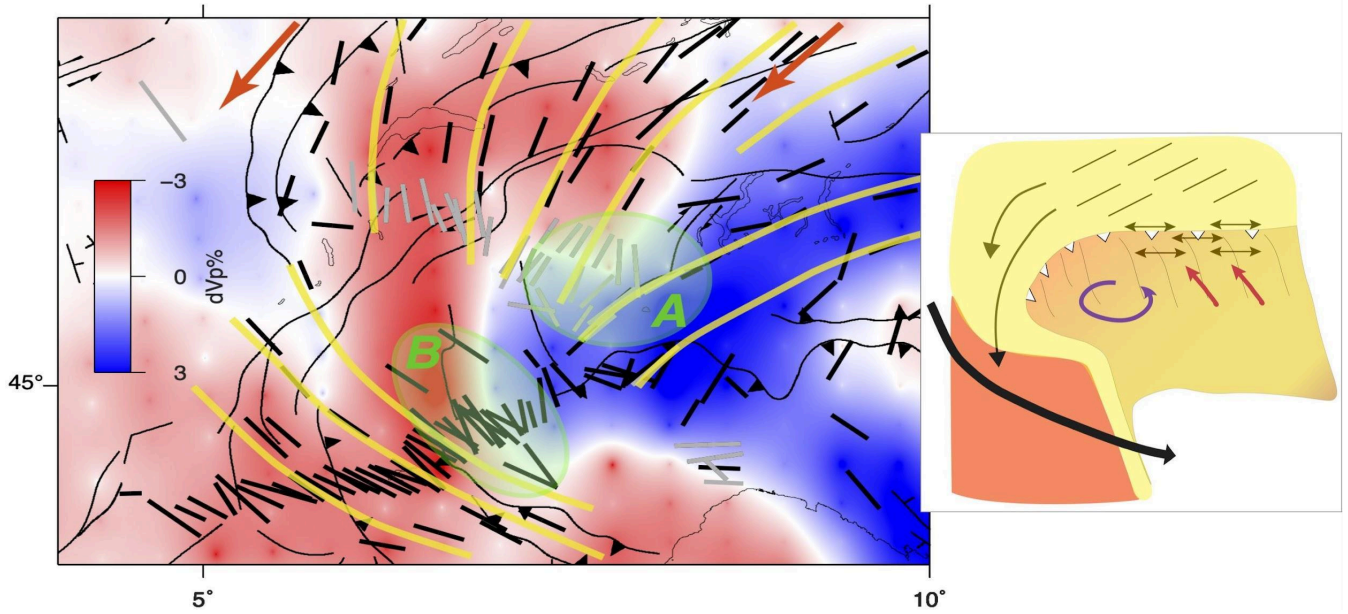

Figure 6 - Left: Zhao et al. (2016) tomography (dVp in %) - layer at 150 km depth - overlapped with average SWS measurements: results from CIFALPS2 data in light grey and from previous studies in black. Orange arrows on top represent the absolute European plate motion from GSRM v2.1 model (calculated from Plate Motion Calculator | Software | GAGE). Yellow traces simulate average mantle deformation directions and green areas A and B highlight points where directions converge. Right: a sketch of this part of alpine subduction, where, in light yellow is the European plate, the double-headed arrows represent the only anisotropy of the study region related to European slab retreat (whose direction is represented by the red arrows), thin black lines are the anisotropy parallel to the APM, the thick black arrow represents the SE France asthenospheric mantle flow, the purple circular arrow represents the Adria plate rotation.

It is worth noting that beneath the Po basin, the European slab is nearly vertical (e.g., Zhao et al. 2016; Paffrath et al., 2021) and the space for the mantle above is really narrow. With such a complex mantle structure, it is not surprising that a unique and significant pattern of anisotropy cannot be identified. In the Ligurian Alps, our measurements show different orientations east and west of the transect with, in general, a prevailing EW direction (Figure 5d), but a minor NNE-SSW set of measurements from the western back azimuths. These results are certainly intriguing but not sufficient to support any new hypothesis.

5 Conclusion

New data collected by the CIFALPS2 project clearly fill the gap that has forced the interpolation between more sparse information in the past. The pattern of seismic anisotropy shown here, is not entirely parallel to the belt, as it is in the Central Alps and in the transition to the Western Alps, up to the point this portion of belt is arcuate. Indeed, in the central part of the study region, a nearly NS pattern coming from central Europe cuts all principal morphologic features of the belt. It converges

with the part of the mantle deformed by the retreating slab in the point where the retreat is less favored or ended. The arcuate shape of the belt and of the slab, added to the Adria plate rotation with respect to Eurasia around a pole here particularly close to the boundary, reduce the effectiveness of a slab retreat. The NS mantle flow is then interpreted as the European mantle moving south to merge with the large asthenospheric flow that from beneath Central France moves toward the Tyrrhenian Sea turning around the southern tip of the European slab.

Data availability

All shear wave splitting measurements from this work have been included and are available in the Italian shear wave splitting collection https://osf.io/nqxk4 (Pondrelli et al., 2023).

Author contribution

PS, SS and CJM made measurements and analyses. PS prepared the manuscript with the contribution of all co-authors. All authors designed the CIFALPS2 experiment and carried it out.

Competing interests

The authors declare that they have no conflict of interest.

Acknowledgements

This research is funded by the National Natural Science Foundation of China and by NEWTON (NEw Window inTO Earth's iNterior), ERC StG funded project (grant ID:758199).

References

Barruol, G., Bonnin, M., Pedersen, H., Bokelmann, G., Tiberi, C.: Belt-parallel mantle flow beneath a halted continental collision: the Western Alps, Earth Planet. Sci. Lett. 302, 429–438, 2011.

Barruol, G., Deschamps, A., Coutant, O.: Mapping upper mantle anisotropy beneath SE France by SKS splitting indicates a Neogene asthenospheric flow induced by the Apenninic slab rollback and deflected by the deep Alpine roots, Tectonophys., 394, 125–138, 2004.

Barruol, G. and M. Granet: A Tertiary asthenospheric flow beneath the southern FrenchMassif Central related to the west Mediterranean extension evidenced by upper mantle seismic anisotropy, Earth Plan. Sci. Lett., 202, 31-47, 10.1016/S0012-821X(02)00752-5, 2002.

Chevrot, S.: Multichannel analysis of shear wave splitting, J. Geophys. Res. Solid Earth, 105(B9), 21579-21590, 2000.

Confal, J. M., Baccheschi, P., Pondrelli, S., Karakostas, F., VanderBeek, B. P., Huang, Z., Faccenda, M.: Reproducing Complex Anisotropy Patterns at Subduction Zones from Splitting Intensity Analysis and Anisotropy Tomography, Geophys. J. Int., 235, 1725–1735, https://doi.org/10.1093/gji/ggad329, 2023.

Crampin, S. and Peacock S.: A review of the current understanding of seismic shear-wave splitting in the Earth's crust and common fallacies in interpretation, Wave Mot., 45 (2008), pp. 675-722, 10.1016/j.wavemoti.2008.01.003, 2008.

Díaz, J., Gil, A., and Gallart, J.: Uppermost mantle seismic velocity and anisotropy in the Euro-Mediterranean region from Pn and Sn tomography, Geophys. J. Int., 192(1), 310-325, 2013.

Monteiller, V., and Chevrot, S.: How to make robust splitting measurements for single-station analysis and three-dimensional imaging of seismic anisotropy, Geophys. J. Int., 182(1), 311-328, 2010.

Giacomuzzi, G., Chiarabba, C., and De Gori, P.: Linking the Alps and Apennines subduction systems: New constraints revealed by high-resolution teleseismic tomography, Earth and Plan. Science Lett., 301(3–4), 531–543, 2011.

Hetényi G., I. Molinari, J. Clinton et al.: The AlpArray Seismic Network: a large-scale European experiment to image the Alpine orogeny, Surv. Geophysics, 39, 1009-1033. doi:10.1007/s10712-018-9472-4, 2018.

Kissling, E., Schmid, S. M., Lippitsch, R., Ansorge, J., and Fügenschuh, B.: Lithosphere structure and tectonic evolution of the Alpine arc: New evidence from high-resolution teleseismic tomography, Geological Society, London, Memoirs, 32, 129–145, 2006.

Kong, F., Gao, S. S., and Liu, K. H.: Applicability of the multiple-event stacking technique for shear-wave splitting analysis, Bull. Seism. Soc. Am., 105(6), 3156-3166, 2015.

Le Breton, E., Handy, M. R., Molli, G., and Ustaszewski, K.: Post-20 Ma motion of the Adriatic plate: New constraints from surrounding Orogens and implications for crust-mantle decoupling, Tectonics, 36, 3135–3154. doi:10.1002/ 2016TC004443, 2017.

Lippitsch, R., Kissling, E., and Ansorge, J.: Upper mantle structure beneath the Alpine orogen from high-resolution teleseismic tomography, J. Geophys. Res.: Solid Earth, 108(B8). https://doi.org/10.1029/2002JB002016, 2003.

Long, M.: Constraints on subduction geodynamics from seismic anisotropy. Rev. Geophys., 51, 76–112, https://doi.org/10.1002/rog.20008, 2013.

Long, M.D., and Silver, P. G.: Shear Wave Splitting and Mantle Anisotropy: Measurements, Interpretations, and New Directions, Surv Geophys 30, 407–461, https://doi.org/10.1007/s10712-009-9075-1, 2009.

Malusà, M. G., C. Faccenna, S. L. Baldwin, P. G. Fitzgerald, F. Rossetti, M. L. Balestrieri, M. Danišík, A. Ellero, G. Ottria, and C. Piromallo: Contrasting styles of (U)HP rock exhumation along the Cenozoic Adria-Europe plate boundary (Western Alps, Calabria, Corsica), Geochem. Geophys. Geosyst., 16, 1786–1824, doi:10.1002/2015GC005767, 2015.

Malusà, M. G., Guillot, S., Zhao, L., Paul, A., Solarino, S., Dumont, T., Schwartz, S., Aubert, C., Baccheschi, P., Eva, E., Lu, Y., Lyu, C., Pondrelli, S., Salimbeni, S., Sun, W., & Yuan, H.: The deep structure of the Alps based on the CIFALPS seismic experiment: A synthesis, Geochem. Geophys. Geosyst., 22(3), e2020GC009466, 2021.

Okaya, D., S.S. Vel, W.J. Song, S.E. Johnson: Modification of crustal seismic anisotropy by geological structures ("structural geometric anisotropy"), Geosphere, 15, pp. 146-170, 10.1130/GES01655, 2018.

Paffrath, M., Friederich, W., Schmid, S. M., Handy, M. R., and AlpArray and AlpArray-Swath D Working Group: Imaging structure and geometry of slabs in the greater Alpine area–A P-wave travel-time tomography using AlpArray Seismic Network data, Solid Earth, 12, 2671-2702, doi: 10.5194/se-12-2671-2021, 2021.

Paul, A., M.G. Malusà, S. Solarino, S. Salimbeni, E. Eva, A. Nouibat, S. Pondrelli, C. Aubert, T. Dumont, S. Guillot, S. Schwartz, L. Zhao: Along-strike variations in the fossil subduction zone of the Western Alps revealed by the CIFALPS seismic experiments and their implications for exhumation of (ultra-) high-pressure rocks, Earth Plan. Science Lett., 598, 117843, https://doi.org/10.1016/j.epsl.2022.117843, 2022.

Piromallo, C., and Morelli, A.: P wave tomography of the mantle under the Alpine-Mediterranean area, J. Geophys. Res.: Solid Earth, 108(B2). https://doi.org/10.1029/2002JB001757, 2003.

Pondrelli S., S. Salimbeni, P. Baccheschi, J. M. Confal, L. Margheriti (2023). Peeking inside the mantle structure beneath the Italian region through SKS shear wave splitting anisotropy: a review, Ann. Geophys., 66, 2, doi:1044.01/ag-8872.

Rappisi, F., VanderBeek, B. P., Faccenda, M., Morelli, A., Molinari, I.: Slab geometry and upper mantle flow patterns in the Central Mediterranean from 3D anisotropic P-wave tomography, J. Geophys. Res.: Solid Earth, 127, e2021JB023488. doi: 10.1029/2021JB023488, 2022.

Reiss, M. C. and G. Rümpker: SplitRacer: MATLAB Code and GUI for Semiautomated Analysis and Interpretation of Teleseismic Shear-Wave Splitting, Seism. Res. Lett., 88, 2A, 392-409, doi: https://doi.org/10.1785/0220160191, 2017.

Salimbeni, S., M. G. Malusà, L. Zhao, S. Guillot, S. Pondrelli, L. Margheriti, A. Paul, S. Solarino, C. Aubert, T. Dumont, S. Schwartz, Q. Wang, X. Xu, T. Zheng and R. Zhu: Active and fossil mantle flows in the western Alpine region unravelled by seismic anisotropy analysis and high-resolution P wave tomography, Tectonophys., 731-732, 35-47, doi:10.1016/j.tecto.2018.03.002, 2018.

Serpelloni, E., G. Vannucci, L. Anderlini, and R.A. Bennett: Kinematics, seismotectonics and seismic potential of the eastern sector of the European Alps from GPS and seismic deformation data, Tectonophys., https://doi.org/10.1016/j.tecto.2016.09.026, 2016.

Silver, P. G. and W. W. Chan: Shear wave splitting and subcontinental mantle deformation, J. Geophys. Res.: Solid Earth, 96, B10, 16429-16454, 1991.

Zhao, L., Paul, A., Guillot, S., Solarino, S., Malusà, M.G., Zheng, T.Y., Aubert, C., Salimbeni, S., Dumont, T., Schwartz, S., Zhu, R.X., Wang, Q.C.: First seismic evidence for continental subduction beneath the Western Alps, Geology 43, 815–818, 2015.

Zhao, L., Paul, A., Malusà, M. G., Xu, X., Zheng, T., Solarino, S., Guillot, S. Schwartz, S., Dumont, T., Salimbeni, S., Aubert, C., Pondrelli, S., Wang, Q., and Zhu, R.: Continuity of the Alpine slab unraveled by high-resolution P wave tomography, J. Geophys. Res., 121, 8720–8737, 2016.

Zhao, L., Paul, A., Solarino, S., RESIF: Seismic network YP: CIFALPS temporary experiment (China-Italy-France Alps seismic transect) [Data set]. RESIF - Réseau Sismologique et géodésique Français. https://doi.org/10.15778/RESIF.YP2012, 2016.

Zhao, L., Paul, A., Solarino, S., RESIF: Seismic network XT: CIFALPS-2 temporary experiment (China-Italy-France Alps seismic transect #2 [Data set]. RESIF - Réseau Sismologique et Géodésique Franc ais. https://doi.org/10.15778/RESIF. XT2018, 2018.

Zhao D., Liu X., Wang Z. and Gou T.: Seismic Anisotropy Tomography and Mantle Dynamics, Surv. Geophys., 44, 947–982, https://doi.org/10.1007/s10712-022-09764-71, 2023.

Supplementary Material

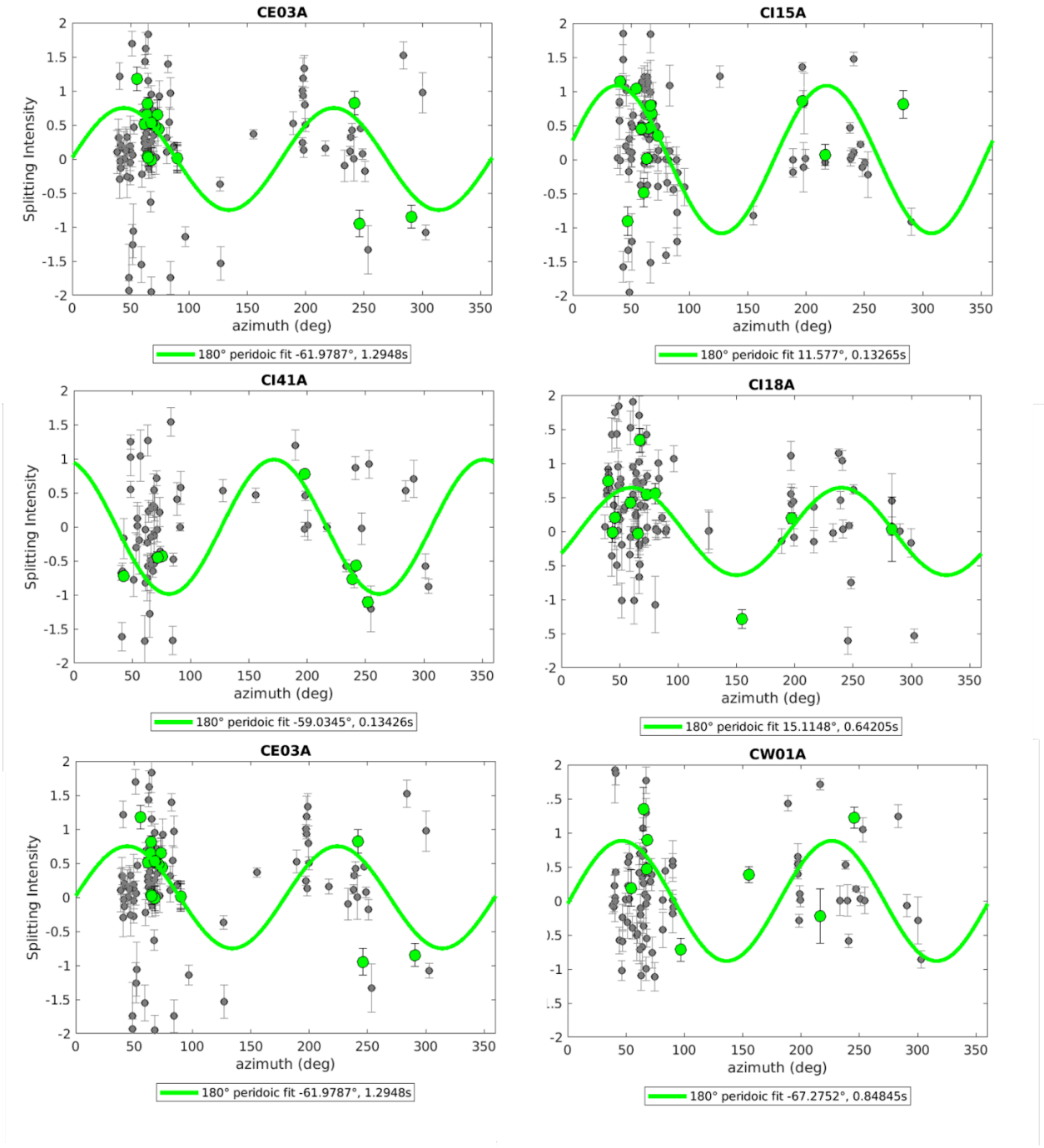

Figure S1 - Splitting intensity measurements for a few example stations. Gray dots: all measurements; green circles: only measurements that fit the criteria and the sinusoidal curve (fast polarization direction and time delay written below).

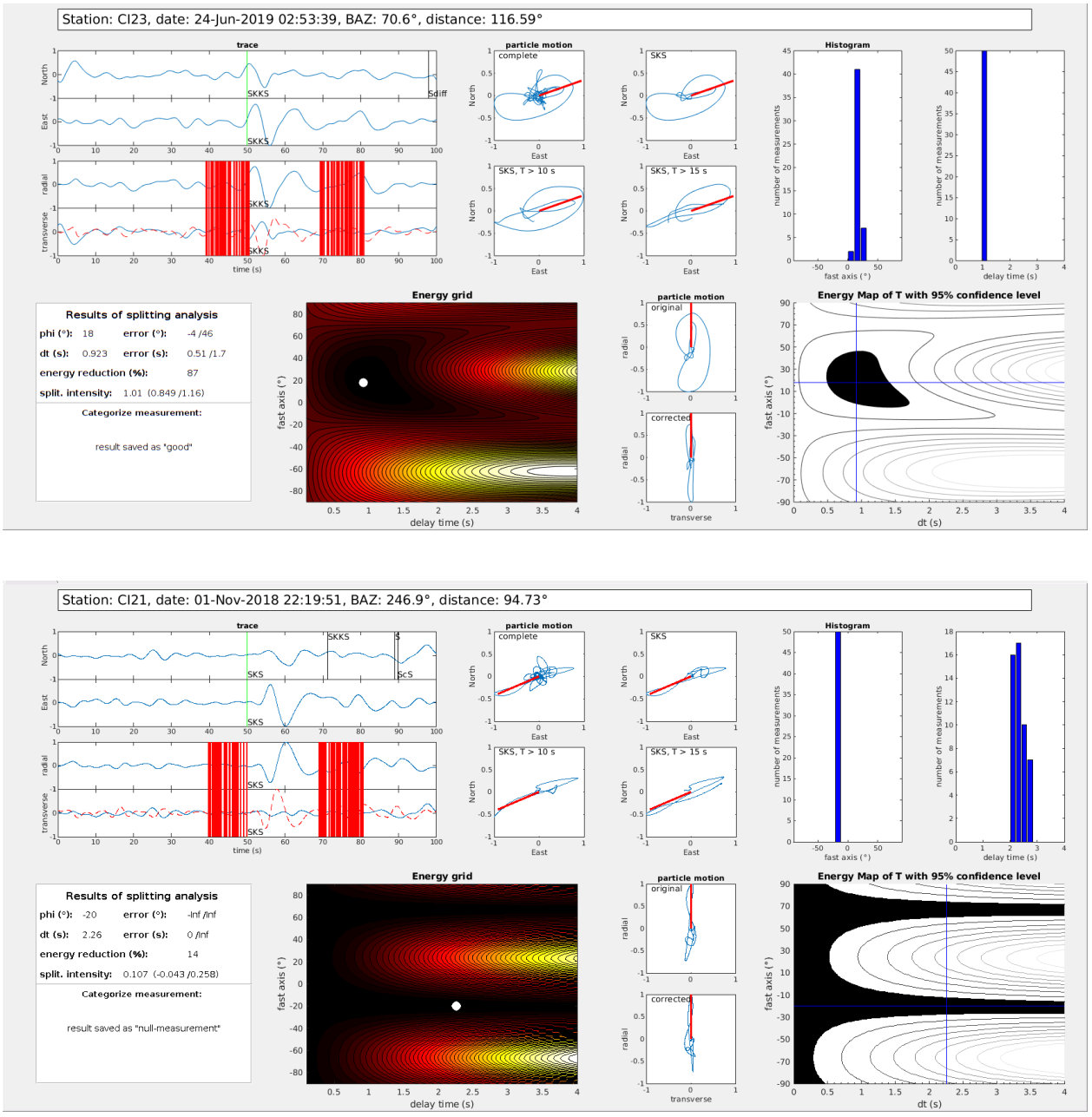

Figure S2 - Examples of measurements. Upper panel: a good shear wave splitting measurement at station CI23. Lower panel: a null measurement at station CI21.

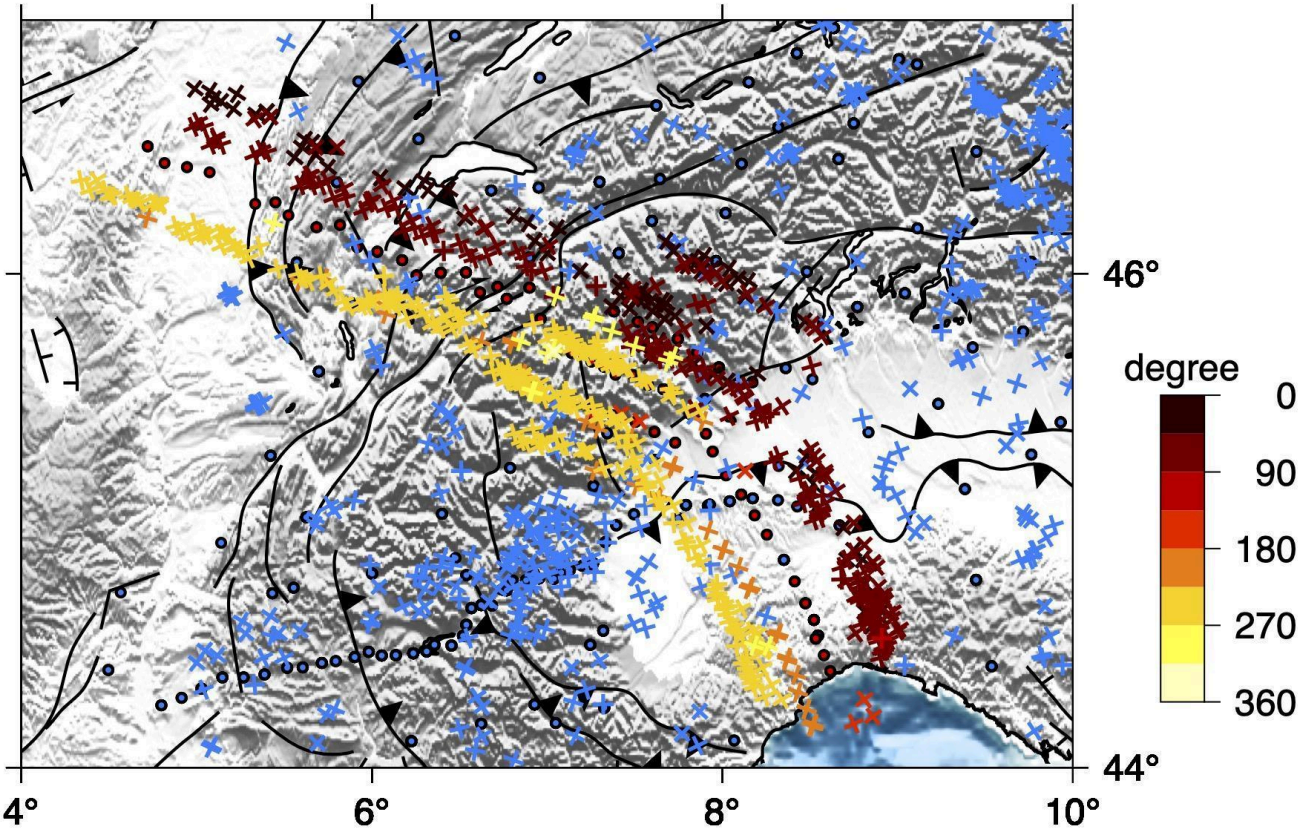

Figure S3 – Map of null measurements plotted at the piercing point of 150 km depth, marked with crosses rotated in the back azimuth direction and coloured following the color scale on the right, depending on the back azimuth; in light blue all previous data.

Table S1 - Good single Splitting Intensity (SI) measurements. Header: Station | Station latitude | Station longitude | Earthquake ID (YYMMDDhhmm) | back-azimuth | SI |SI error

Station	Lat	Lon	EQ ID	BAZ	SI	SI error
CE01	45.85	7.38	1809281002	73.70	0.56	0.04
CE01	45.85	7.38	1812290339	64.00	0.06	0.09
CE01	45.85	7.38	1901061727	66.54	0.65	0.04
CE01	45.85	7.38	1901171506	52.65	0.75	0.26
CE01	45.85	7.38	1901260812	66.06	-0.16	0.18
CE01	45.85	7.38	1903150503	245.84	0.39	0.15
CE01	45.85	7.38	1904121140	72.66	0.44	0.07
CE01	45.85	7.38	1904230537	61.60	0.43	0.06
CE01	45.85	7.38	1905141258	46.67	1.24	0.09
CE01	45.85	7.38	1905311012	64.11	0.31	0.13
CE01	45.85	7.38	1907071508	68.18	0.24	0.23
CE01	45.85	7.38	1907140943	67.84	-0.40	0.38
CE01	45.85	7.38	1909190706	83.83	0.62	0.06
CE01	45.85	7.38	1909211953	69.62	0.01	0.17
CE01	45.85	7.38	1909252346	69.16	0.32	0.17
CE01	45.85	7.38	1910290104	64.96	1.83	0.16
CE01	45.85	7.38	1911141617	67.24	1.11	0.06
CE02	45.81	7.52	1809281025	74.30	1.92	0.28
CE02	45.81	7.52	1901212359	81.62	-0.54	0.23
CE02	45.81	7.52	1902121234	40.73	-0.08	0.28
CE02	45.81	7.52	1904121140	72.78	0.74	0.36

CE02	45.81	7.52	1906240253	70.77	0.85	0.03
CE02	45.81	7.52	1907140539	86.98	0.35	0.35
CE02	45.81	7.52	1907140943	67.97	-0.62	0.27
CE02	45.81	7.52	1908021203	89.90	0.01	0.12
CE02	45.81	7.52	1909190706	83.94	1.09	0.06
CE02	45.81	7.52	1910290104	65.08	1.86	0.18
CE03	45.79	7.60	1809281002	73.89	0.44	0.04
CE03	45.79	7.60	1812290339	64.19	0.65	0.03
CE03	45.79	7.60	1901181640	290.91	-0.85	0.17
CE03	45.79	7.60	1902020927	90.21	0.02	0.18
CE03	45.79	7.60	1902021059	90.19	0.02	0.22
CE03	45.79	7.60	1902021101	89.97	0.02	0.20
CE03	45.79	7.60	1903150503	246.00	-0.95	0.19
CE03	45.79	7.60	1904121140	72.86	0.65	0.23
CE03	45.79	7.60	1904230537	61.78	0.51	0.07
CE03	45.79	7.60	1905062119	55.46	1.18	0.17
CE03	45.79	7.60	1905311012	64.30	0.04	0.08
CE03	45.79	7.60	1906140019	241.68	0.82	0.17
CE03	45.79	7.60	1906240253	70.85	0.49	0.06
CE03	45.79	7.60	1907071508	68.38	0.53	0.04
CE03	45.79	7.60	1909141621	67.50	-0.01	0.18
CE03	45.79	7.60	1909290202	64.64	0.81	0.09
CE03	45.79	7.60	1910161137	65.18	0.02	0.13
CE03	45.79	7.60	1911141617	67.44	0.54	0.06
CE04	45.74	7.75	1809281002	74.01	0.90	0.08

CE04	45.74	7.75	1812290339	64.32	0.49	0.04
CE04	45.74	7.75	1901061727	66.87	1.22	0.13
CE04	45.74	7.75	1904220911	63.38	-0.06	0.13
CE04	45.74	7.75	1904230537	61.90	0.66	0.04
CE04	45.74	7.75	1905311012	64.42	0.62	0.04
CE04	45.74	7.75	1906240253	70.99	0.49	0.03
CE04	45.74	7.75	1907071508	68.51	0.82	0.08
CE04	45.74	7.75	1909190706	84.12	0.48	0.06
CE04	45.74	7.75	1909290202	64.76	1.31	0.12
CE04	45.74	7.75	1910290104	65.27	0.73	0.08
CE04	45.74	7.75	1910310111	65.04	-0.39	0.24
CE04	45.74	7.75	1911052052	189.30	0.79	0.21
CE04	45.74	7.75	1911150117	67.63	1.83	0.26
CE05	45.68	7.86	1810292017	216.72	0.37	0.12
CE05	45.68	7.86	1811040755	65.60	0.10	0.18
CE05	45.68	7.86	1812290339	64.42	0.34	0.05
CE05	45.68	7.86	1902081155	62.14	0.41	0.21
CE05	45.68	7.86	1903240437	67.67	0.50	0.31
CE05	45.68	7.86	1904121140	73.09	1.03	0.06
CE05	45.68	7.86	1904230537	61.99	1.00	0.05
CE05	45.68	7.86	1905311012	64.52	0.77	0.27
CE05	45.68	7.86	1906240253	71.10	0.75	0.04
CE05	45.68	7.86	1907071508	68.61	1.37	0.08
CE05	45.68	7.86	1909290202	64.86	1.55	0.14
CE05	45.68	7.86	1910310111	65.14	1.42	0.09

CE05	45.68	7.86	1911141617	67.68	0.28	0.15
CE06	45.63	7.98	1812290339	64.54	0.58	0.08
CE06	45.63	7.98	1901171506	53.37	1.42	0.22
CE06	45.63	7.98	1903010850	251.39	1.21	0.10
CE06	45.63	7.98	1904062155	74.88	-0.16	0.07
CE06	45.63	7.98	1904121140	73.20	0.68	0.06
CE06	45.63	7.98	1904230537	62.10	0.66	0.08
CE06	45.63	7.98	1906240253	71.23	1.27	0.03
CE06	45.63	7.98	1907011659	64.54	1.01	0.20
CE06	45.63	7.98	1907071508	68.73	1.48	0.05
CE06	45.63	7.98	1907081852	68.65	0.96	0.09
CE06	45.63	7.98	1907140943	68.41	1.43	0.37
CE06	45.63	7.98	1907141026	68.08	-1.18	0.07
CE06	45.63	7.98	1911141617	67.79	1.26	0.05
CE07	45.57	8.17	1809281002	74.38	0.77	0.11
CE07	45.57	8.17	1812110226	198.19	-0.23	0.06
CE07	45.57	8.17	1812290339	64.70	0.95	0.08
CE07	45.57	8.17	1904050956	41.09	0.61	0.26
CE07	45.57	8.17	1904230537	62.25	0.35	0.07
CE07	45.57	8.17	1906040439	41.36	-0.27	0.10
CE07	45.57	8.17	1907011659	64.70	0.20	0.44
CE07	45.57	8.17	1907071508	68.91	0.78	0.09
CE07	45.57	8.17	1907141026	68.25	1.83	0.13
CI01	46.50	4.72	1809281014	71.35	-1.19	0.12
CI01	46.50	4.72	1901221901	153.32	0.65	0.11

CI01	46.50	4.72	1902020927	88.08	0.90	0.14
CI02	46.44	4.82	1809181157	40.67	0.00	0.09
CI02	46.44	4.82	1809281014	71.45	-1.35	0.08
CI02	46.44	4.82	1810260905	37.16	1.27	0.46
CI02	46.44	4.82	1812011327	69.30	0.00	0.05
CI02	46.44	4.82	1812192137	47.80	0.46	0.12
CI02	46.44	4.82	1901221901	153.39	1.11	0.09
CI03	46.42	4.95	1809281002	71.64	0.28	0.04
CI03	46.42	4.95	1809281014	71.55	-1.57	0.22
CI03	46.42	4.95	1809281025	72.11	-1.37	0.18
CI03	46.42	4.95	1904091753	196.05	1.38	0.07
CI03	46.42	4.95	1904220911	61.24	-0.06	0.12
CI04	46.40	5.07	1901221901	153.56	-0.52	0.16
CI04	46.40	5.07	1902121234	38.50	1.47	0.24
CI05	46.28	5.33	1809281025	72.46	1.21	0.16
CI05	46.28	5.33	1903240437	65.43	0.03	0.12
CI05	46.28	5.33	1908272355	196.24	0.27	0.08
CI05	46.28	5.33	1910290242	63.18	-0.02	0.11
CI05	46.28	5.33	1911231211	60.00	0.24	0.13
CI06	46.28	5.45	1901212359	79.84	0.40	0.08
CI06	46.28	5.45	1906040439	39.28	0.34	0.05
CI06	46.28	5.45	1907141026	65.75	-0.92	0.42
CI06	46.28	5.45	1911042153	238.70	0.03	0.15
CI07	46.23	5.52	1810020016	79.26	-0.42	0.17
CI07	46.23	5.52	1810292326	282.59	-0.02	0.20

CI07	46.23	5.52	1812160942	57.14	0.55	0.10
CI07	46.23	5.52	1901181640	289.41	0.00	0.04
CI07	46.23	5.52	1901200132	240.02	0.03	0.33
CI07	46.23	5.52	1901212359	79.92	0.01	0.18
CI07	46.23	5.52	1901220510	80.09	0.01	0.18
CI07	46.23	5.52	1901221901	153.87	0.00	0.06
CI07	46.23	5.52	1901260812	64.23	0.03	0.34
CI07	46.23	5.52	1901301531	282.22	0.01	0.06
CI07	46.23	5.52	1902020927	88.69	0.01	0.13
CI07	46.23	5.52	1902021059	88.67	0.01	0.13
CI07	46.23	5.52	1902021101	88.44	0.01	0.13
CI07	46.23	5.52	1902081155	60.18	0.04	0.43
CI07	46.23	5.52	1904062155	72.64	0.20	0.05
CI07	46.23	5.52	1907141026	65.84	-0.70	0.24
CI07	46.23	5.52	1911042153	238.74	1.88	0.45
CI08	46.18	5.68	1810260905	38.00	0.47	0.08
CI08	46.18	5.68	1811011930	196.58	1.32	0.12
CI08	46.18	5.68	1901220510	80.24	-0.66	0.08
CI08	46.18	5.68	1901260351	42.14	0.83	0.30
CI08	46.18	5.68	1907141026	65.99	-0.54	0.29
CI08	46.18	5.68	1909290202	62.99	1.21	0.32
CI08	46.18	5.68	1911161019	65.86	0.26	0.19
CI09	46.19	5.82	1809230552	42.15	-0.47	0.19
CI09	46.19	5.82	1812011327	70.27	-0.60	0.10
CI09	46.19	5.82	1901220510	80.34	-0.85	0.08

CI09	46.19	5.82	1903060013	60.97	0.69	0.13
CI09	46.19	5.82	1904051614	198.90	-0.01	0.12
CI09	46.19	5.82	1911141845	66.04	-1.48	0.33
CI10	46.11	5.92	1809281002	72.50	0.17	0.04
CI10	46.11	5.92	1812110226	197.10	1.31	0.07
CI10	46.11	5.92	1812280303	61.53	0.21	0.15
CI10	46.11	5.92	1901200132	240.25	0.02	0.25
CI10	46.11	5.92	1909190732	82.63	-0.44	0.04
CI11	46.09	6.03	1809181157	42.41	0.02	0.10
CI11	46.09	6.03	1810292326	282.94	0.24	0.31
CI11	46.09	6.03	1811011930	196.75	0.75	0.30
CI11	46.09	6.03	1812110226	197.16	1.04	0.09
CI11	46.09	6.03	1901212359	80.37	0.09	0.07
CI11	46.09	6.03	1902021059	89.05	-0.90	0.19
CI11	46.09	6.03	1905162252	282.79	0.54	0.17
CI11	46.09	6.03	1906040439	39.73	0.68	0.24
CI11	46.09	6.03	1907071508	67.01	0.69	0.03
CI12	46.05	6.17	1812110226	197.23	1.06	0.11
CI12	46.05	6.17	1812290339	62.97	0.03	0.04
CI12	46.05	6.17	1901260351	42.81	0.93	0.17
CI12	46.05	6.17	1905162252	282.89	1.74	0.33
CI12	46.05	6.17	1906040439	39.84	0.67	0.07
CI12	46.05	6.17	1906240253	69.53	0.50	0.05
CI12	46.05	6.17	1907071508	67.13	0.70	0.03
CI12	46.05	6.17	1910290104	63.96	0.44	0.06

CI12	46.05	6.17	1910310111	63.72	1.00	0.13
CI13	45.99	6.26	1809281014	72.70	1.80	0.17
CI13	45.99	6.26	1810102200	46.90	-0.34	0.24
CI13	45.99	6.26	1812290339	63.06	0.01	0.09
CI13	45.99	6.26	1901260351	42.95	0.80	0.10
CI13	45.99	6.26	1906040439	39.90	1.02	0.08
CI14	46.00	6.39	1809281025	73.37	1.72	0.49
CI14	46.00	6.39	1811040755	64.40	0.89	0.18
CI14	46.00	6.39	1901061727	65.69	1.04	0.11
CI14	46.00	6.39	1901221901	154.45	-0.78	0.08
CI14	46.00	6.39	1904051614	199.19	-0.05	0.21
CI14	46.00	6.39	1904221449	198.79	0.10	0.17
CI14	46.00	6.39	1911141845	66.57	-0.04	0.20
CI15	46.01	6.54	1809281002	73.01	0.35	0.03
CI15	46.01	6.54	1810102200	47.20	-0.91	0.21
CI15	46.01	6.54	1810290654	216.44	0.07	0.15
CI15	46.01	6.54	1812290339	63.28	0.02	0.08
CI15	46.01	6.54	1901260812	65.24	0.46	0.12
CI15	46.01	6.54	1902081155	61.04	-0.48	0.21
CI15	46.01	6.54	1905062119	54.23	1.04	0.07
CI15	46.01	6.54	1905162252	283.15	0.81	0.20
CI15	46.01	6.54	1906191724	58.74	0.45	0.09
CI15	46.01	6.54	1906281551	40.68	1.15	0.03
CI15	46.01	6.54	1907071508	67.44	0.68	0.06
CI15	46.01	6.54	1908272355	196.79	0.85	0.03

CI15	46.01	6.54	1911141617	66.51	0.80	0.04
CI16	45.92	6.62	1809281002	73.09	0.62	0.04
CI16	45.92	6.62	1809281025	73.57	-0.49	0.16
CI16	45.92	6.62	1812190137	253.14	-0.03	0.25
CI16	45.92	6.62	1901221901	154.61	-0.01	0.06
CI16	45.92	6.62	1901260812	65.35	0.03	0.32
CI16	45.92	6.62	1901301531	282.96	0.01	0.06
CI16	45.92	6.62	1902020927	89.50	0.01	0.13
CI16	45.92	6.62	1902021059	89.48	0.01	0.13
CI16	45.92	6.62	1902021101	89.26	0.01	0.13
CI16	45.92	6.62	1902081155	61.11	0.05	0.40
CI16	45.92	6.62	1903081506	61.23	1.55	0.19
CI16	45.92	6.62	1904230537	60.99	1.01	0.05
CI16	45.92	6.62	1905062119	54.37	0.99	0.07
CI16	45.92	6.62	1905141258	45.78	0.87	0.19
CI16	45.92	6.62	1906040439	40.18	0.97	0.07
CI16	45.92	6.62	1906191724	58.85	1.38	0.11
CI16	45.92	6.62	1906240253	69.96	0.59	0.06
CI16	45.92	6.62	1906281551	40.76	1.33	0.05
CI16	45.92	6.62	1907071508	67.54	0.87	0.04
CI16	45.92	6.62	1907140910	66.78	1.30	0.11
CI16	45.92	6.62	1907141026	66.86	1.09	0.21
CI16	45.92	6.62	1908272355	196.83	1.32	0.05
CI16	45.92	6.62	1910290844	44.71	-0.28	0.10
CI17	45.95	6.72	1809281002	73.16	0.45	0.07

CI17	45.95	6.72	1810020016	80.31	1.45	0.23
CI17	45.95	6.72	1810101844	82.37	-0.09	0.11
CI17	45.95	6.72	1812290339	63.44	0.03	0.14
CI17	45.95	6.72	1901181640	290.27	-0.68	0.13
CI17	45.95	6.72	1901200132	240.73	0.38	0.11
CI17	45.95	6.72	1901221901	154.67	-0.92	0.10
CI17	45.95	6.72	1901301531	283.04	0.80	0.11
CI17	45.95	6.72	1902121234	40.02	0.45	0.26
CI17	45.95	6.72	1903041006	53.47	1.24	0.44
CI17	45.95	6.72	1903081506	61.30	0.65	0.09
CI17	45.95	6.72	1904091753	196.91	0.41	0.10
CI17	45.95	6.72	1906040439	40.25	0.73	0.07
CI17	45.95	6.72	1906281551	40.85	0.82	0.03
CI17	45.95	6.72	1907071508	67.61	0.70	0.03
CI17	45.95	6.72	1909190706	83.31	0.84	0.05
CI17	45.95	6.72	1910161137	64.44	0.37	0.08
CI18	45.90	6.77	1809281002	73.22	0.54	0.07
CI18	45.90	6.77	1810012359	80.36	0.55	0.15
CI18	45.90	6.77	1812110226	197.51	0.19	0.08
CI18	45.90	6.77	1901221901	154.71	-1.29	0.14
CI18	45.90	6.77	1901260351	43.62	-0.01	0.15
CI18	45.90	6.77	1901260812	65.50	-0.03	0.35
CI18	45.90	6.77	1901301531	283.07	0.03	0.47
CI18	45.90	6.77	1902121234	40.07	0.74	0.17
CI18	45.90	6.77	1902171435	46.02	0.20	0.31

CI18	45.90	6.77	1906191724	59.00	0.42	0.09
CI18	45.90	6.77	1907140910	66.91	1.34	0.18
CI19	45.94	6.90	1812192137	50.38	-0.86	0.19
CI19	45.94	6.90	1903010850	250.64	0.52	0.05
CI19	45.94	6.90	1904051614	199.46	1.10	0.08
CI19	45.94	6.90	1904062155	73.88	1.87	0.14
CI19	45.94	6.90	1904091753	197.00	0.26	0.20
CI19	45.94	6.90	1904121140	72.25	0.77	0.06
CI19	45.94	6.90	1906040439	40.39	1.24	0.13
CI19	45.94	6.90	1906191724	59.10	1.39	0.08
CI19	45.94	6.90	1907071508	67.76	0.94	0.04
CI19	45.94	6.90	1908272355	196.96	0.72	0.04
CI19	45.94	6.90	1909291557	237.91	0.79	0.07
CI19	45.94	6.90	1911141617	66.82	1.58	0.05
CI21	45.72	7.14	1809280659	73.71	0.41	0.34
CI21	45.72	7.14	1809281002	73.55	1.08	0.10
CI21	45.72	7.14	1809281014	73.46	1.54	0.09
CI21	45.72	7.14	1810141241	126.72	0.04	0.17
CI21	45.72	7.14	1812290339	63.84	0.84	0.08
CI21	45.72	7.14	1901181640	290.55	0.07	0.38
CI21	45.72	7.14	1901212359	81.37	0.15	0.23
CI21	45.72	7.14	1901220510	81.54	0.26	0.19
CI21	45.72	7.14	1901260351	44.17	0.94	0.26
CI21	45.72	7.14	1906240253	70.49	0.97	0.04
CI21	45.72	7.14	1907071508	68.03	1.11	0.05

CI21	45.72	7.14	1907140539	86.75	1.16	0.12
CI21	45.72	7.14	1909141621	67.14	-0.09	0.16
CI21	45.72	7.14	1909190732	83.64	1.50	0.26
CI21	45.72	7.14	1911150117	67.15	-1.21	0.14
CI22	45.68	7.14	1809281002	73.56	0.80	0.07
CI22	45.68	7.14	1809281014	73.47	1.94	0.20
CI22	45.68	7.14	1905162252	283.51	-0.04	0.16
CI22	45.68	7.14	1907011659	63.88	1.96	0.14
CI22	45.68	7.14	1907071508	68.04	0.97	0.09
CI22	45.68	7.14	1907140539	86.77	0.92	0.16
CI23	45.68	7.24	1809281002	73.64	1.07	0.07
CI23	45.68	7.24	1810020016	80.83	-0.37	0.17
CI23	45.68	7.24	1810141241	126.79	-1.21	0.16
CI23	45.68	7.24	1812160942	59.06	-0.01	0.06
CI23	45.68	7.24	1812161426	96.66	-0.02	0.25
CI23	45.68	7.24	1812290339	63.93	0.39	0.06
CI23	45.68	7.24	1901061727	66.48	0.46	0.10
CI23	45.68	7.24	1901181640	290.62	-0.91	0.21
CI23	45.68	7.24	1903060013	62.22	0.48	0.08
CI23	45.68	7.24	1904051614	199.61	0.04	0.14
CI23	45.68	7.24	1904230537	61.52	0.86	0.06
CI23	45.68	7.24	1905030725	39.67	1.39	0.16
CI23	45.68	7.24	1905311012	64.03	0.60	0.07
CI23	45.68	7.24	1906240253	70.60	0.95	0.04
CI23	45.68	7.24	1907071508	68.12	0.90	0.05

CI23	45.68	7.24	1910290104	64.89	0.79	0.08
CI23	45.68	7.24	1911141617	67.18	1.19	0.13
CI24	45.65	7.25	1809281002	73.66	1.07	0.09
CI24	45.65	7.25	1812290339	63.95	0.31	0.05
CI24	45.65	7.25	1902021101	89.73	-0.33	0.24
CI24	45.65	7.25	1904062155	74.29	0.19	0.09
CI24	45.65	7.25	1904230537	61.53	0.86	0.05
CI24	45.65	7.25	1905062119	55.19	0.07	0.30
CI24	45.65	7.25	1906240253	70.62	1.03	0.05
CI24	45.65	7.25	1907071508	68.14	0.90	0.05
CI24	45.65	7.25	1910142223	90.32	1.03	0.06
CI24	45.65	7.25	1910290104	64.90	0.92	0.06
CI24	45.65	7.25	1911052052	189.03	-0.24	0.25
CI24	45.65	7.25	1911231211	61.89	0.55	0.07
CI25	45.63	7.32	1809281002	73.72	0.97	0.07
CI25	45.63	7.32	1809281025	74.20	0.64	0.14
CI25	45.63	7.32	1812290339	64.01	0.44	0.04
CI25	45.63	7.32	1901220510	81.72	0.98	0.08
CI25	45.63	7.32	1902121234	40.60	-0.19	0.13
CI25	45.63	7.32	1903041006	54.27	-0.55	0.14
CI25	45.63	7.32	1904230537	61.59	0.57	0.05
CI25	45.63	7.32	1905311012	64.11	-1.80	0.38
CI25	45.63	7.32	1906240253	70.69	1.04	0.06
CI25	45.63	7.32	1907071508	68.21	0.91	0.10
CI25	45.63	7.32	1907141026	67.54	-0.92	0.19

CI25	45.63	7.32	1910290104	64.96	1.17	0.13
CI25	45.63	7.32	1911141617	67.27	0.27	0.08
CI26	45.60	7.39	1901220510	81.78	1.15	0.21
CI26	45.60	7.39	1903101248	51.72	0.71	0.28
CI26	45.60	7.39	1907071508	68.27	1.17	0.08
CI26	45.60	7.39	1907141026	67.61	1.75	0.45
CI27	45.60	7.49	1810020016	81.05	0.39	0.48
CI28	45.56	7.57	1904230537	61.79	0.45	0.11
CI28	45.56	7.57	1907140943	68.10	1.42	0.38
CI29	45.54	7.66	1905311012	64.41	0.44	0.24
CI29	45.54	7.66	1906240253	71.01	1.09	0.15
CI29	45.54	7.66	1907071508	68.51	0.79	0.39
CI29	45.54	7.66	1905311012	64.41	0.44	0.24
CI29	45.54	7.66	1906240253	71.01	1.09	0.15
CI29	45.54	7.66	1907071508	68.51	0.79	0.39
CI30	45.52	7.71	1812192137	51.51	-1.19	0.25
CI30	45.52	7.71	1902121234	40.95	-1.45	0.16
CI30	45.52	7.71	1907071508	68.55	1.23	0.11
CI30	45.52	7.71	1909141621	67.68	0.49	0.29
CI31	45.44	7.81	1903010850	251.27	0.58	0.05
CI31	45.44	7.81	1904220911	63.45	0.23	0.11
CI31	45.44	7.81	1906040439	41.09	-0.65	0.15
CI31	45.44	7.81	1910161137	65.42	0.49	0.08
CI32	45.36	7.91	1810102113	50.39	-0.81	0.23
CI32	45.36	7.91	1905311012	64.64	0.74	0.20

CI32	45.36	7.91	1907011659	64.53	-1.09	0.26
CI32	45.36	7.91	1910290104	65.48	0.46	0.14
CI33	45.29	7.94	1812161426	97.32	-0.93	0.12
CI33	45.29	7.94	1901200132	241.36	0.65	0.14
CI33	45.29	7.94	1902021101	90.25	1.85	0.19
CI33	45.29	7.94	1902081155	62.28	0.27	0.09
CI33	45.29	7.94	1906281551	41.99	-1.47	0.07
CI33	45.29	7.94	1907141026	68.17	0.08	0.40
CI34	45.19	8.02	1810102045	50.26	1.44	0.13
CI34	45.19	8.02	1901301531	283.79	0.19	0.18
CI34	45.19	8.02	1906040439	41.26	-0.86	0.13
CI35	45.11	8.11	1811040755	65.91	-0.89	0.11
CI35	45.11	8.11	1911021808	199.25	-0.63	0.14
CI36	45.03	8.18	1810020016	81.81	-1.17	0.24
CI36	45.03	8.18	1901220510	82.60	-0.71	0.07
CI36	45.03	8.18	1902020927	90.67	-0.09	0.23
CI36	45.03	8.18	1904230537	62.34	0.38	0.07
CI36	45.03	8.18	1905311012	64.94	0.82	0.12
CI37	44.95	8.25	1812161426	97.69	-1.46	0.41
CI37	44.95	8.25	1902121234	41.51	0.00	0.13
CI37	44.95	8.25	1903150503	246.43	-0.63	0.14
CI37	44.95	8.25	1905311012	65.01	0.37	0.18
CI37	44.95	8.25	1907150821	52.80	-0.92	0.11
CI37	44.95	8.25	1909141621	68.34	0.77	0.30
CI37	44.95	8.25	1910161137	65.87	0.04	0.09

CI38	44.76	8.41	1810290654	216.76	0.00	0.02
CI38	44.76	8.41	1810292017	216.62	0.00	0.02
CI38	44.76	8.41	1810292326	284.31	-0.02	0.16
CI38	44.76	8.41	1903010850	251.66	-0.51	0.05
CI38	44.76	8.41	1904230537	62.56	0.04	0.11
CI38	44.76	8.41	1905311012	65.18	-1.31	0.20
CI38	44.76	8.41	1906250601	127.59	0.01	0.06
CI38	44.76	8.41	1906281551	42.47	-0.01	0.09
CI38	44.76	8.41	1907011659	65.02	-0.02	0.24
CI38	44.76	8.41	1907071508	69.35	-0.02	0.24
CI38	44.76	8.41	1907081852	69.27	-0.02	0.23
CI38	44.76	8.41	1907122042	63.50	-0.02	0.18
CI38	44.76	8.41	1907140910	68.66	-0.02	0.23
CI38	44.76	8.41	1907140943	69.06	-0.02	0.23
CI38	44.76	8.41	1907141026	68.73	-0.02	0.23
CI38	44.76	8.41	1907150821	53.09	-0.01	0.12
CI38	44.76	8.41	1910290104	66.01	-0.06	0.37
CI38	44.76	8.41	1910290242	65.95	-0.03	0.37
CI38	44.76	8.41	1910310111	65.77	-0.02	0.36
CI38	44.76	8.41	1911021808	199.38	0.00	0.04
CI38	44.76	8.41	1911042153	240.19	-0.02	0.21
CI38	44.76	8.41	1911052052	189.62	0.00	0.03
CI38	44.76	8.41	1911141845	68.58	-0.03	0.42
CI38	44.76	8.41	1911142112	68.46	-0.38	0.41
CI38	44.76	8.41	1911150117	68.46	-0.03	0.43

CI38	44.76	8.41	1911161019	68.50	-0.02	0.42
CI38	44.76	8.41	1911231211	63.20	-0.03	0.31
CI38	44.76	8.41	1912030846	249.30	-0.03	0.34
CI39	44.67	8.47	1810290654	216.75	-1.12	0.15
CI39	44.67	8.47	1810292326	284.33	1.74	0.24
CI39	44.67	8.47	1902020927	90.90	0.09	0.30
CI39	44.67	8.47	1907140943	69.14	1.87	0.44
CI39	44.67	8.47	1908272355	197.59	0.92	0.03
CI39	44.67	8.47	1911231211	63.28	-0.20	0.15
CI40	44.60	8.52	1902020927	90.94	-1.97	0.25
CI40	44.60	8.52	1904221449	199.78	0.30	0.38
CI40	44.60	8.52	1906191724	61.22	-0.75	0.07
CI40	44.60	8.52	1907140539	88.35	-0.78	0.23
CI40	44.60	8.52	1909141621	68.68	0.27	0.22
CI41	44.53	8.53	1903010850	251.73	-1.10	0.07
CI41	44.53	8.53	1904062155	75.78	-0.43	0.06
CI41	44.53	8.53	1906140019	241.98	-0.57	0.04
CI41	44.53	8.53	1906240253	72.19	-0.45	0.08
CI41	44.53	8.53	1906281551	42.61	-0.73	0.04
CI41	44.53	8.53	1908272355	197.60	0.78	0.02
CI41	44.53	8.53	1909291557	238.46	-0.77	0.04
CI42	44.46	8.58	1901220510	83.12	1.14	0.23
CI42	44.46	8.58	1901221901	155.96	0.87	0.05
CI42	44.46	8.58	1903150503	246.65	-1.35	0.20
CI42	44.46	8.58	1906240253	72.26	-0.60	0.10

CI42	44.46	8.58	1909291557	238.47	-1.21	0.07
CI42	44.46	8.58	1911142112	68.69	-0.49	0.05
CI43	44.40	8.62	1811011930	197.91	-0.01	0.12
CI43	44.40	8.62	1811040755	66.44	0.03	0.27
CI43	44.40	8.62	1901221901	155.98	0.95	0.07
CI43	44.40	8.62	1902171435	48.88	-0.70	0.10
CI43	44.40	8.62	1903010850	251.79	-0.70	0.09
CI43	44.40	8.62	1906240253	72.32	-0.32	0.06
CI43	44.40	8.62	1908011828	238.95	-0.88	0.07
CI43	44.40	8.62	1909190706	85.08	-1.42	0.09
CI43	44.40	8.62	1909291557	238.47	-1.08	0.08
CW01	45.43	7.26	1810292017	216.40	-0.22	0.40
CW01	45.43	7.26	1811040755	65.19	1.35	0.32
CW01	45.43	7.26	1812161426	96.79	-0.72	0.17
CW01	45.43	7.26	1901221901	155.05	0.39	0.12
CW01	45.43	7.26	1903041006	54.32	0.19	0.27
CW01	45.43	7.26	1903150503	245.75	1.23	0.15
CW01	45.43	7.26	1907071508	68.22	0.89	0.05
CW01	45.43	7.26	1907141026	67.56	0.47	0.10
CW02	45.43	7.37	1810290654	216.58	1.77	0.12
CW02	45.43	7.37	1810292017	216.45	-0.22	0.10
CW02	45.43	7.37	1901181640	290.69	-1.46	0.48
CW02	45.43	7.37	1902121234	40.67	-0.78	0.12
CW02	45.43	7.37	1906250601	126.80	-1.91	0.19
CW02	45.43	7.37	1907071508	68.31	1.07	0.09

CW02	45.43	7.37	1908142135	302.99	-0.04	0.36
CW02	45.43	7.37	1909141621	67.44	0.04	0.19
CW03	45.41	7.51	1901061727	66.77	1.73	0.20
CW03	45.41	7.51	1904230537	61.76	0.59	0.08
CW03	45.41	7.51	1907071508	68.42	0.86	0.10
CW03	45.41	7.51	1910290104	65.16	-0.58	0.20
CW04	45.37	7.61	1810292326	283.91	-1.01	0.31
CW04	45.37	7.61	1903060013	62.58	0.44	0.09
CW04	45.37	7.61	1907071508	68.52	1.08	0.09
CW05	45.32	7.73	1901260812	66.63	0.87	0.11
CW05	45.32	7.73	1910290104	65.35	-0.71	0.09
CW05	45.32	7.73	1911052052	189.28	1.43	0.38

Table S2 - Splitting parameters for stations with good SI measurements from at least four different back-azimuthal bin directions. Header: Station | Station latitude (Lat) | Station longitude (Lon) | FPD | FPDerr | TD | TDerr | RMS | Number of Measurements (#)

Station	Lat	Lon	FPD	FPDerr	TD	TDerr	RMS	#
CE03	45.79	7.60	-0.78	2.35	0.75	0.06	12.64	18
CI07	46.23	5.52	11.58	6.57	0.13	0.04	8.05	17
CI11	46.09	6.03	-0.33	1.56	0.83	0.05	13.30	9
CI15	46.01	6.54	-7.45	0.57	1.08	0.02	18.86	13
CI16	45.92	6.62	-2.58	0.66	1.09	0.02	27.78	23
CI17	45.95	6.72	11.48	0.96	0.79	0.02	17.21	17
CI18	45.90	6.77	15.11	2.53	0.64	0.06	8.29	11
CI19	45.94	6.90	0.98	0.61	1.32	0.03	20.85	12
CI21	45.72	7.14	37.08	2.27	1.04	0.07	18.74	15
CI23	45.68	7.24	22.22	1.97	0.74	0.05	20.34	17
CI24	45.65	7.25	37.75	1.59	0.93	0.05	14.58	12
CI37	44.95	8.25	87.15	12.30	0.32	0.09	9.52	7
CI38	44.76	8.41	-59.03	3.69	0.13	0.02	10.61	28
CI39	44.67	8.47	-43.54	2.80	1.01	0.07	16.59	6
CI41	44.53	8.53	-53.46	0.62	0.99	0.02	19.35	7
CI42	44.46	8.58	76.64	1.76	2.18	0.13	5.75	6
CI43	44.40	8.62	-67.28	1.86	0.85	0.06	12.82	9
CW01	45.43	7.26	1.35	3.98	0.88	0.13	12.19	8
CW02	45.43	7.37	22.80	2.92	0.78	0.08	19.64	8